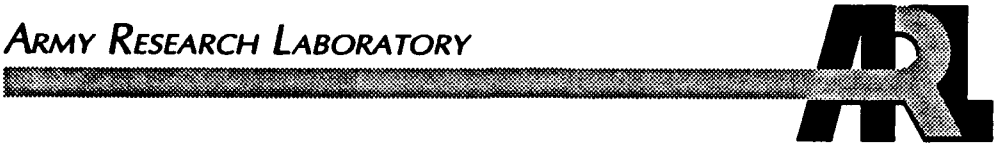

Structural Analysis of a Cannon-Caliber Electromagnetic Projectile

Lawrence W. Burton

ARL-TR-214 September 1993

Original contains color plates: All DTIC reproductions will be in black and white

NOTICES

Destroy this report when it is no longer needed. DO NOT return it to the originator.

Additional copies of this report may be obtained from the National Technical Information Service, U.S. Department of Commerce, 5285 Port Royal Road, Springfield, VA 22161.

The findings of this report are not to be construed as an official Department of the Army position, unless so designated by other authorized documents.

The use of trade names or manufacturers' names in this report does not constitute indorsement of any commercial product.

DISCLAIMER NOTICE

THIS DOCUMENT IS BEST QUALITY AVAILABLE. THE COPY FURNISHED TO DTIC CONTAINED A SIGNIFICANT NUMBER OF COLOR PAGES WHICH DO NOT REPRODUCE LEGIBLY ON BLACK AND WHITE MICROFICHE.

REPORT DOCUMENTATION PAGE

Form Approved
OMB No. 0704-0188

1. AGENCY USE ONLY (Leave blank)	2. REPORT DATE	3. REPORT TYPE AND DATES COVERED
	September 1993	Final, Jun 92 - Feb 93

4. TITLE AND SUBTITLE
Structural Analysis of a Cannon-Caliber Electromagnetic Projectile

5. FUNDING NUMBERS
PR: 1L162618AH80

6. AUTHOR(S)
Lawrence W. Burton

7. PERFORMING ORGANIZATION NAME(S) AND ADDRESS(ES)
U.S. Army Research Laboratory
ATTN: AMSRL-WT-PD
Aberdeen Proving Ground, MD 21005-5066

8. PERFORMING ORGANIZATION REPORT NUMBER

9. SPONSORING / MONITORING AGENCY NAME(S) AND ADDRESS(ES)
U.S. Army Research Laboratory
ATTN: AMSRL-OP-CI-B (Tech Lib)
Aberdeen Proving Ground, MD 21005-5066

10. SPONSORING / MONITORING AGENCY REPORT NUMBER
ARL-TR-214

11. SUPPLEMENTARY NOTES

12a. DISTRIBUTION / AVAILABILITY STATEMENT
Approved for public release; distribution is unlimited.

12b. DISTRIBUTION CODE

13. ABSTRACT (Maximum 200 words)

An electromagnetic (EM) projectile design is evaluated by adopting finite element procedures similar to those employed in the analysis of kinetic energy (KE) projectiles from conventional cannons. The specific assumptions required to tailor the analysis to the unique aspects of the EM system are detailed. Quasi-static analysis runs are made for two different acceleration levels and are used to compare against the results of five transient analyses having various loading profiles. Lastly, recommendations are left for the EM projectile designer of specific areas of concern which must be examined in future projectile analysis.

14. SUBJECT TERMS
electromagnetic projectiles, transient analysis, finite element procedures, projectiles, finite element analysis

15. NUMBER OF PAGES
36

16. PRICE CODE

17. SECURITY CLASSIFICATION OF REPORT	18. SECURITY CLASSIFICATION OF THIS PAGE	19. SECURITY CLASSIFICATION OF ABSTRACT	20. LIMITATION OF ABSTRACT
UNCLASSIFIED	UNCLASSIFIED	UNCLASSIFIED	UL

INTENTIONALLY LEFT BLANK.

ACKNOWLEDGMENTS

The author would like to extend his appreciation to Mr. Alexander Zielinski for his work in formulating the acceleration loading profiles utilized for the transient analyses. Thanks is also extended for his assistance and guidance in assuring the representation of the loading conditions in the analyses was an accurate reflection of that found in an EM railgun. Finally, both Mr. Alexander Zielinski and Mr. James Bender are thanked for their critique and review of this report during its preparation.

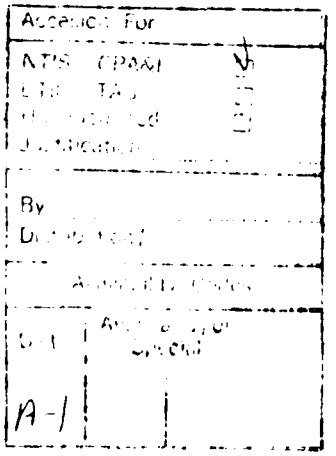

INTENTIONALLY LEFT BLANK.

TABLE OF CONTENTS

INTENTIONALLY LEFT BLANK.

LIST OF FIGURES

INTENTIONALLY LEFT BLANK.

1. INTRODUCTION

Over the past decade, finite element (FE) analysis of a conventionally launched projectile subjected to pressure loading has become a necessary step in the munition design process. A methodology has been developed which allows for a two-dimensional, quasi-static analysis, that is, a static balance between peak pressure and a resisting body force acceleration. Techniques for simplified modeling of threaded interfaces, fins, and nosetips have also been formulated.

Electromagnetic (EM) railguns differ from conventional propellant gun systems in that they do not use a pressure load on the surface of a projectile as the propulsion force, but a body force acceleration, provided by current conducted through a solid armature in a magnetic field. The mode of operation of EM guns has been detailed elsewhere, and the interested reader is encouraged to review the information presented in the literature (Price et al. 1987; Jamison and Burden 1989; Mongeau 1990).

While EM guns and gas pressure guns are different, the means of examining a projectile's structural integrity are the same. Various assumptions are required when modeling the projectile geometry to allow for a two-dimensional quasi-static analysis. Many of the techniques validated in previous projectile analyses of conventional gun systems have application in EM projectile analysis and will be utilized here. The details of these modeling assumptions and the results of the subsequent analysis will be a primary focus of this report.

One concern unique to the EM projectile designer is the shortened rise time of the force loading in comparison to that of gas pressure. While this capability may be beneficial by allowing for shorter barrel lengths, it may possibly introduce stress waves to the structure leading to elevated stress states that may be catastrophic. A quasi-static analysis would fail to account for these dynamic effects. Thus, when dealing with reduced rise times it is important to perform a transient dynamic analysis. The commercially available FE code ANSYS (DeSalvo and Gorman 1989) was used for the analyses detailed in this report because of its ability to determine structural response under time-dependent loading. Five different load profiles were considered for the transient analysis. The initial static analysis utilized the two peak loadings from the five load profiles. Ultimately, the influence of pulse shape is assessed as a function of the projectile stress-state.

It is important to point out that this work was performed with the intention of developing a generic EM projectile design and analysis methodology using finite element techniques. The projectile modeled served only as a vehicle on which to refine the modeling technique, with the analysis not intended to produce a design with tactical applications.

2. PROJECTILE DESIGN AND MODELING

The projectile design under consideration is the result of a design study to support the Cannon Caliber Electromagnetic Launcher (CCEML) effort. The methodology used to attain an integrated launch package design considers the target performance at range and was first used for the 0.60-cal. armor-piercing fin-stabilized discarding armature (APFSDA) projectile package (Zielinski 1991). Subsequent to that analysis, the methodology was applied to a cannon-caliber type launcher (Zielinski 1990). The design procedure uses static, simplified mechanical analysis to determine rod and armature structural integrity.

The selected APFSDA configuration which satisfied the CCEML performance requirements has a 23-mm bore diameter, a 0.194-lb (88-g) launch mass, and a muzzle velocity of 7,710 ft/s (2,350 m/s). Also, the analysis assumed a sinusoidal current pulse, with the half-cycle terminated at the end of the 2-m barrel length (Zielinski 1993).

A plastic-composite fin assembly with four blades attached was incorporated in the design to provide a means of flight stabilization. Figure 1 shows a complete assembly of the EM projectile. A dimensioned drawing of the sabot/armature is shown in Figure 2. Note, the integrated launch package is not axisymmetric. To simplify the analysis and keep it two-dimensional, it was decided to adjust the density of the asymmetric armature over its rear 0.9 in (2.3 cm). The resultant density was 65% that of aluminum and allowed for this rear portion of the armature to be modeled as a cylinder. The specific calculations for determining this value are presented in the Appendix. Figures 3 and 4 are provided to show the geometries of the penetrator and fin hub, respectively.

A few other assumptions were made to simplify the geometry of the FE model. The mass of the fin blades was lumped into the fin hub to allow for cylindrical modeling of the tail section. A similar approach was taken in squaring off the penetrator nose. In both cases, the length of the cylindrical masses was chosen to keep the center of gravity of the entire structure from shifting.

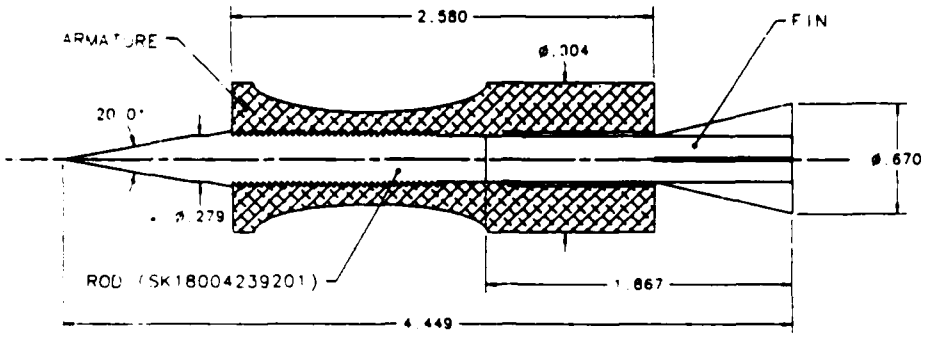

Figure 1. Assembly drawing of EM projectile.

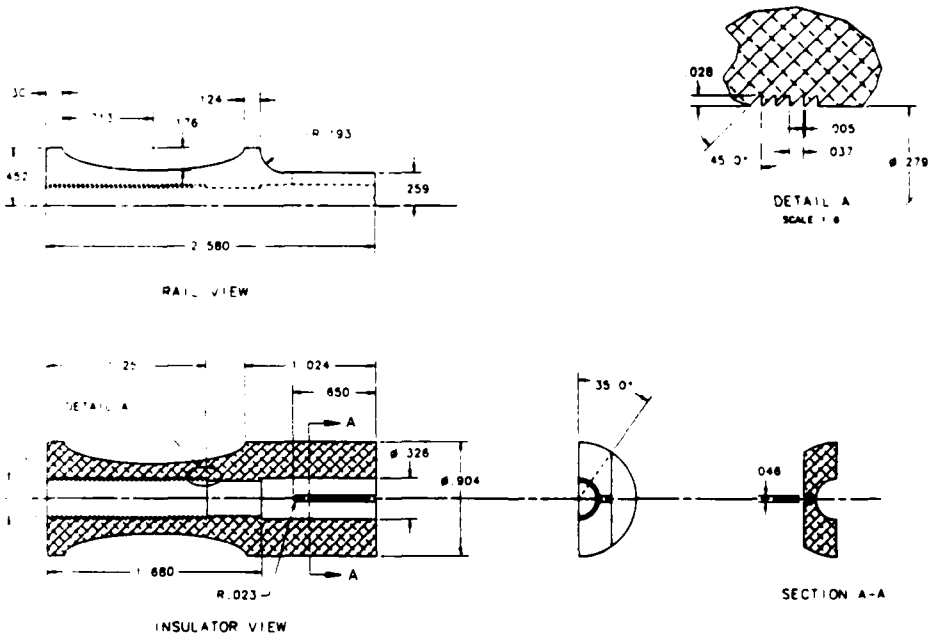

Figure 2. Dimensioned drawing of sabot/armature.

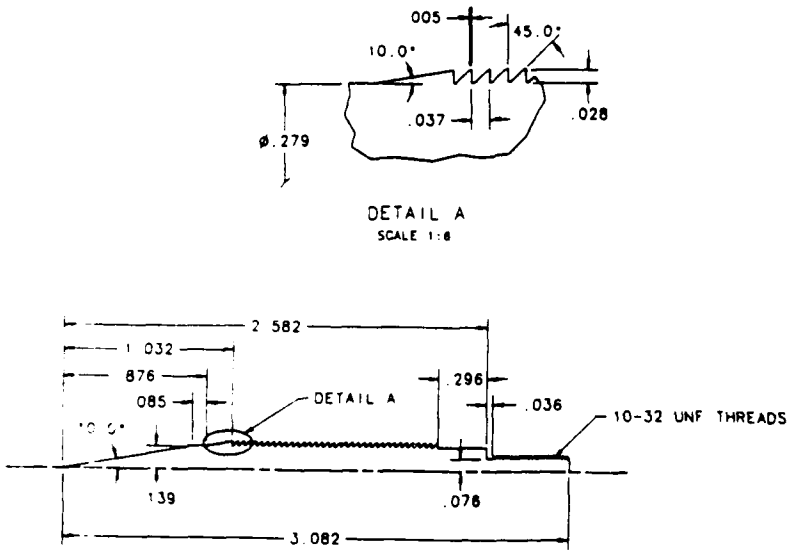

Figure 3. Tungsten penetrator of 23-mm projectile.

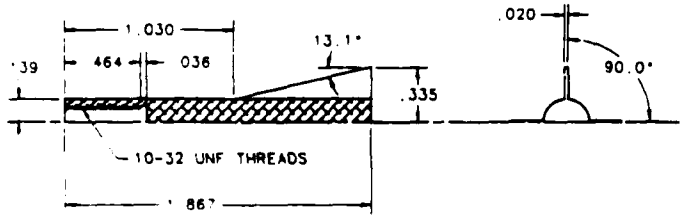

Figure 4. 23-mm projectile fin hub geometry.

Initially, it was decided to model each of the 34 teeth of the penetrator and sabot along their interface. Figure 5 shows the grid pattern used for each groove, with 16 elements utilized in both penetrator and sabot. Nodes were shared between the penetrator and sabot along the driving flank of each tooth and are therefore, in effect, bonded. A 0.001-in (0.00254-cm) gap was modeled between the nondriving surfaces of the teeth.

The rear nongrooved interface of the penetrator and sabot was modeled with gap elements provided in the ANSYS code which allow for sliding and opening along the interface. It is important not to bond the nodes between these two structures because this would provide an additional driving surface and allow for stress relief of the armature via additional load being carried by the tungsten core.

The final decision to be made for the modeling effort concerned the way to represent the EM loading. Previous analytical work has shown that the current density through the armature is concentrated heavily towards the rear of the armature (Powell, Walbert, and Zielinski 1993). While ANSYS has the capability of placing internal force loads within a structure, it was decided to adopt a simplified approach. Therefore, the approach adopted applied a pressure along the back surface of the armature to provide a force equivalent to the actual EM load. It was desired to investigate two different load cases, one providing a peak force of 39,500 lbf (176 kN) and a second having a peak of 52,600 lbf (234 kN). Newton's Second Law of Motion was used to calculate accelerations of 201,000 and 268,000 g's for the two cases. The applied pressures were calculated by dividing the previous peak forces by the area of the armature over which the pressure is to be applied. The resultant pressure values used in the FE analysis were 70,860 psi (489 MPa) for the less severe load case and 94,212 psi (650 MPa) for the high load case.

The final modeled geometry of the projectile is displayed in Figure 6. There are more than 3,300 elements due to the detailed modeling of the grooved interface region. Radial constraints were placed along the top of the sabot/armature to represent the presence of the gun barrel. This geometry model, with the less severe load case (176 kN), was used to begin the analysis.

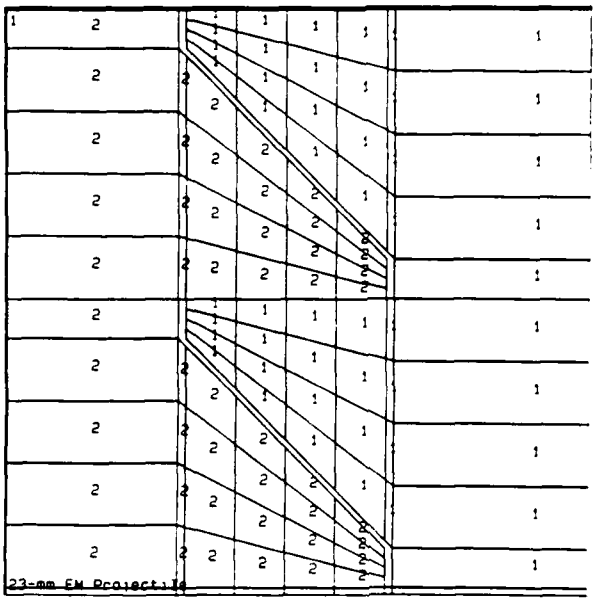

Figure 5. Element grid geometry of penetrator/sabot interface.

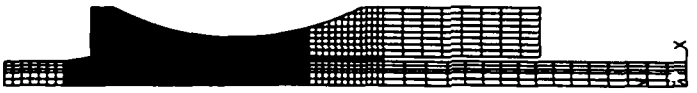

Figure 6. FE model of 23-mm projectile.

3. RESULTS OF THE PRELIMINARY ANALYSIS

The initial analysis of the projectile described in the previous section showed extremely high stresses in the rear teeth of the penetrator/sabot interface. The model also experienced numerical convergence problems associated with the use of gap elements. The material properties of the aluminum were extended to include the plastic regime to allow deformation in an attempt to reduce stresses. Also, the ANSYS manual suggested that ramping the load to its peak value would aid in the convergence of the gap elements, and this advice was followed (DeSalvo and Gorman 1989). The mass of the model was calculated by the code to be 0.196 lb (89 g), which agreed with the previously calculated value and provided confidence that the geometry model of the projectile was correct (Zielinski 1990).

With multiple load steps and a plasticity model for the aluminum incorporated, the model was rerun. Again, the results showed excessive stress levels in the rear teeth, but the sabot exhibited severe deformation with convergence of the gap elements achieved. This information led to efforts to reduce the stresses present in the projectile.

At this point in the analysis effort, a hardware problem was encountered with the computer system in use. The FE work had been performed on a RISC-based processor in a HP730 workstation. This system has the ability to process 76 *million instructions per second* (MIPS). An analysis of the EM projectile with plasticity material models, gap elements, and multiple load steps required approximately 8 1/2 hours to complete. With this system down, the available alternative was a Motorola-based processor on an Apollo ring, capable of processing 7.5 MIPS. Thus, continuing on with the present model would have taken at least 10 times longer to perform an analysis run than on the HP machine. Facing the prospect of a 3-1/2 day run per quasi-static run on the slower system and with even lengthier runs resulting from transient analyses, it was decided to modify the grid of the FE model.

First, the grooved interface was modeled using a material that represented the tungsten-aluminum mated teeth. This material was given a density equal to one-half the sum of the densities of tungsten and aluminum to represent this interface to maintain a correct projectile mass. The material was then given an elastic modulus equal to that of aluminum since this is the less stiff of the two materials which comprise the interface region. This procedure has become commonplace in the analysis of conventional, gas pressure loaded, projectile analysis (Sorensen 1991). Adoption of these assumptions for the grooved interface allowed for the use of a much coarser mesh.

Another decision made to reduce the complexity of the analysis, and subsequently reduce run time, was to cease with the use of gap elements along the nongrooved penetrator/armature interface, thereby eliminating the need to perform multiple load steps. Instead, the elements in this region were given very small values for the elastic modulus in the radial direction. This was done so as not to allow for the transfer of load from the armature to the penetrator and artificially reduce the stress level.

The modifications previously outlined were incorporated, the analysis was continued on the Apollo ring, and the results mirrored those obtained previously. Again, the rear tooth region showed excessive stress levels with plastic deformation of the sabot leading to the belief that the new model on the new machine was consistent with the work done previously. Therefore, efforts were initiated to reduce the stress state.

4. ANALYSIS OF THE MODIFIED PROJECTILE

It was felt that increasing the length of the grooved interface would greatly reduce the magnitude of the stress contours through the projectile. Therefore, the length of the grooves was extended to span the entire length of the penetrator/sabot surface. The convention of employing an adjusted material for the annular grooves was continued and eliminated the need to reduce the modulus of material along the rear of the interface as had been previously assumed. The plasticity material model was also dropped.

The results of this analysis showed that the stress contours had been reduced to acceptable levels. A color plot is shown in Figure 7 with the stress levels listed at the right and given in pounds per square inch (psi). The maximum stress in the rod is seen to be 157 ksi (1,080 MPa), well below its yield value of 246 ksi (1,690 MPa). A look at the aluminum sabot shows a maximum through effective von Mises stress of 54 ksi (370 MPa), also well below its yield value of 82 ksi (565 MPa). The stresses in the axial direction were seen, as expected, to be approximately 70 ksi (483 MPa), the applied pressure load. The maximum effective stress value does not have as high a level as the applied pressure due to the radial constraints imposed on the boreriders which assists in spreading the load to the hoop direction. An elastic-plastic analysis of the redesign was also performed with little change to the stress values, which is as expected since the stress levels fell well short of the material elastic limits.

Another case which increased the length of the grooved interface over that of the original design but left 0.13 in (0.33 cm) ungrooved at the rear was run. For this case, the maximum effective stress in the

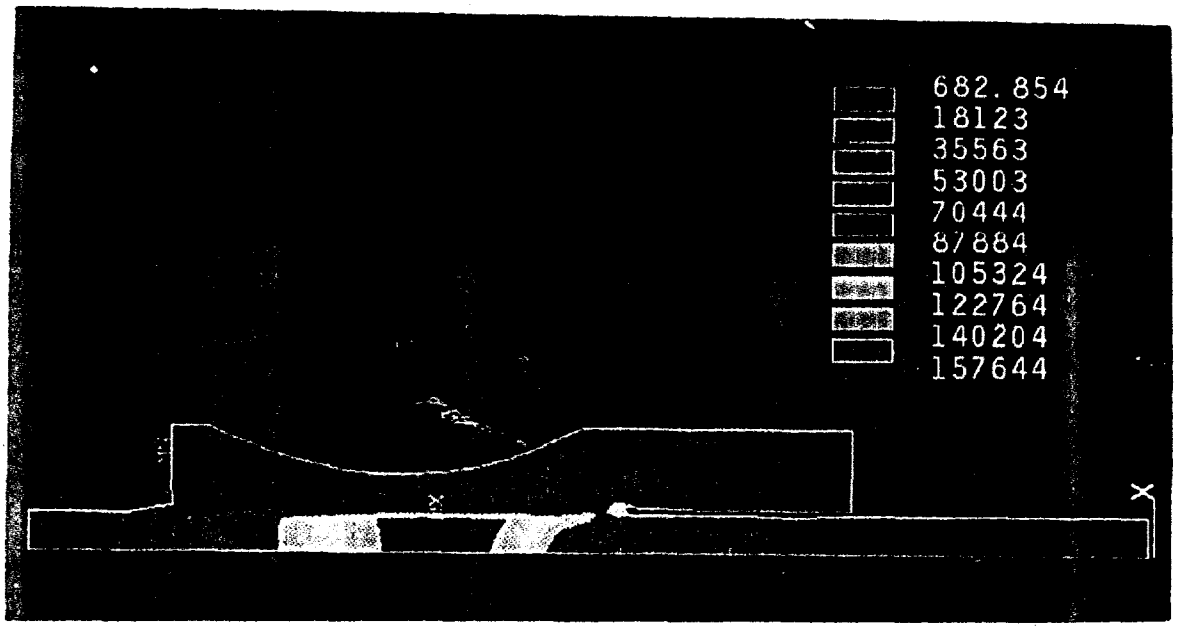

Figure 7 Stress contours in 23-mm projectile with peak force of 176 kN

penetrator remained at 157 ksi (1,080 MPa), but the sabot through stress rose 20%. Thus, it was decided to stay with the fully grooved interface design for the high load case.

The more severe load profile resulted in a peak stress of 210 ksi (1,448 MPa) across the rod with a maximum through stress contour of 72 ksi (496 MPa) in the sabot. A contour plot of the projectile stress levels is shown in Figure 8, with Figure 9 providing a blown-up view of the sabot/armature. Again, these are effective von Mises stress values. Examination of axial stress levels along the rear of the armature exceeded 95 ksi (655 MPa). Once again, the explanation for the difference between effective and axial stress values lies in the boundary condition assumption of no radial displacement on the bore-riding surface which assists in loading the projectile in the hoop direction. There is, however, a concern about the boundary condition assumption employed, which is the same as that typically used in the analysis of gas pressure launches. For an EM launch, the magnetic field in the barrel tends to cause the rails to separate (Zielinski, Kezerian, and Beno 1988), thus freeing the armature to move radially outward. Another point to note from Figure 9 is the large compression stress along the base of the armature at the rear of the interface. Part of the reason for this localized high stress is the square geometry of the model in this region as well as the very small element size used to model the geometry. This area of stress

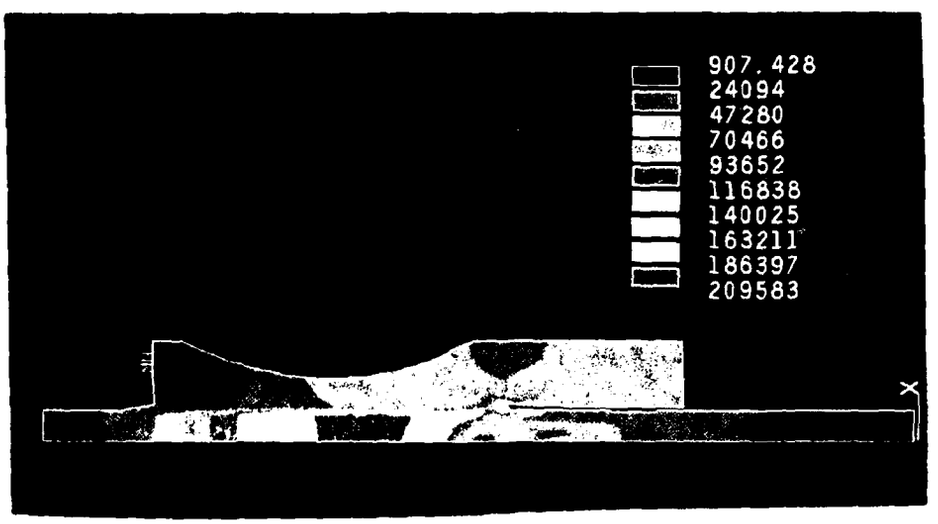
907.428
24094
47280
70466
93652
116838
140025
163211
186397
209583

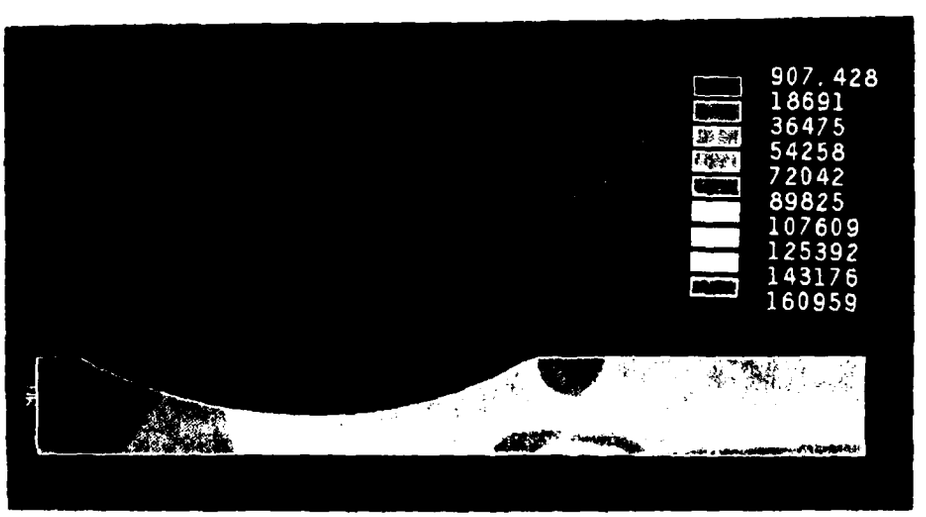
907.428
18691
36475
54258
72042
89825
107609
125392
143176
160959

concentration is something which could be handled by a change in geometry of the design. Since the scope of this effort is on development of the analysis techniques and not on design techniques, no physical changes were made. In an actual design effort, this stress concentration would need to be further addressed.

Another case of the high load profile was run with the radial boundary constraint removed, providing the armature with complete freedom of outward movement. While it is recognized that this too is not an accurate physical model (the rails do provide some restriction on the armature's radial motion), it was felt that this case, accompanied with the previous one, would bracket the range of possible armature motion and the stresses which result. Lacking a true representation of the rail separation, this was felt to be the best approach.

The results of the unconstrained case are shown in Figure 10, and not unexpectedly, the effective stress through the armature has risen appreciably to 92.5 ksi (638 MPa), a 27% increase. The lack of a radial constraint reduces the load carrying capability in the hoop direction. This also causes an increase in the penetrator stress to 223 ksi (1,538 MPa). This then points up the importance of establishing realistic boundary conditions when performing the FE analysis. A poor choice of boundary conditions can lead to a projectile which lacks sufficient robustness to withstand launch conditions being deemed acceptable. This highlights the point that the FE codes are tools which provide results only as accurate as the physical reality of the input.

5. TRANSIENT ANALYSIS

Previous work has shown the shorter rise times typical of EM launches can lead to an amplification of the stress levels due to the generation of stress waves (Bannister, Burton, and Drysdale 1991). While that work focused on a lengthier projectile subjected to a much shorter rise time loading than the cases under consideration here for the 23-mm projectile, it remains important to consider the effects of stress waves for projectile loadings whose rise times approach the time required for these waves to sufficiently dampen out. A saboted projectile is an undamped system, thus requiring a stress wave to traverse the length of the penetrator numerous times before attaining a steady-state value approaching zero. Work done investigating stress waves through bare rods showed that rise times greater than five times the transit time, the time required for a pulse to travel down the length of the penetrator and back, were of sufficient duration to ensure sufficient damping of the stress waves (Bender 1989).

Following Page Intentionally Left Blank

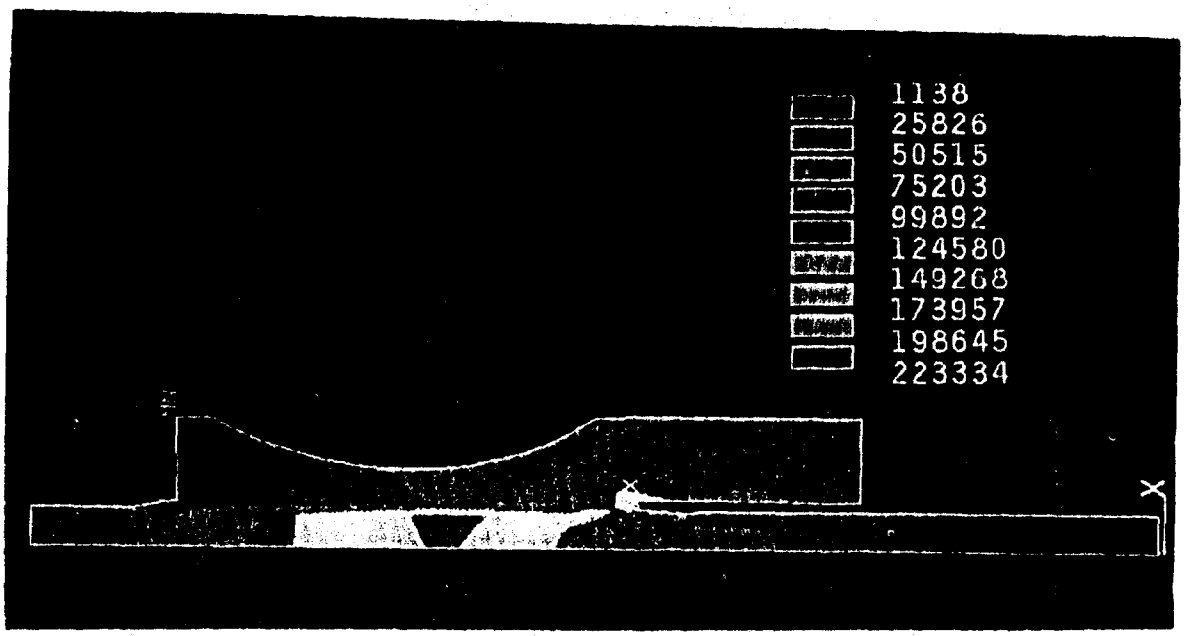

Figure 10. Stress contours in sabot/armature with peak force of 2.34 kN with no radial boundary constraint

The loading profiles for the 25 mm projectile analysis had rise times at least nine times that of the transit, so no problem was anticipated with axial stress waves. However, it was decided to go through the exercise of performing the transient analysis and present it here for completeness of the analysis technique and to ensure that certain modes of vibration are not excited by rise times greater than the transit time but less than those considered static).

Five different loading profiles that varied in magnitude, rise time, and duration were to be investigated because the current profile in an EM gun can significantly alter the amount of energy storage required. Typically, large and fast loadings are desirable for high pulse power electrical efficiency. Conversely, structural integrity is best achieved with relatively soft and slow loadings (Zielinski 1992). Only the total muzzle (89 g and 2,350 m/s) energy remained constant for all five load cases. The acceleration vs. time plots of the five profiles are shown in Figure 11. Table 1 lists the magnitude of peak acceleration, the time of this peak, and the time of projectile exit from a 2 m long gun barrel. Because currents in pulsed power systems can also decay very quickly, an effort was made to assess a wide range of realistic loading profiles.

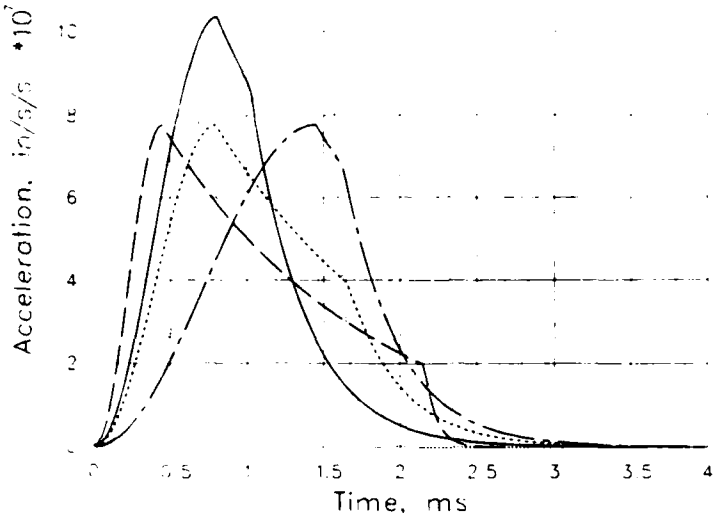

Figure 11. Plots of acceleration profiles used as loading conditions.

Table 1. Acceleration Profile Parameters

Acceleration Case No.	Peak Acceleration (g)	Time of Peak Acceleration (ms)	Time of Travel to Muzzle exit (ms)
1	268,000	0.80	3.55
2	268,000	1.45	8.025
3	201,000	0.45	2.70
4	201,000	0.80	5.50
5	201,000	1.45	4.25

The acceleration profiles were resolved to pressure values every 25 μs, which determined the number of ramped load steps used in the FE run. For instance, case 3 had a muzzle exit time of 0.0027 s, which results in 108 load steps (0.0027/0.000025). The other important consideration for the transient analysis was selection of an integration time step which is established by the selection of the number of iterations per load step. The ANSYS code suggests guidelines to ensure the integration time step is sufficiently small to resolve the motion of the structure, as well as account for possible wave propagation (Desalvo

and Gorman 1989). Using the ANSYS criteria, a value of 0.1 μs was chosen as the integration time step. This then provided for 250 iterations per load step in the FE code.

Having deemed a very small time step necessary, it was decided to derive another FE model of the projectile geometry utilizing a coarser grid to reduce the time required to perform a single analysis run. The model was reduced from 733 elements to 287 elements and rerun with a quasi-static pressure load. There was no appreciable difference in the stress contours between these two models, so the more coarsely gridded projectile was carried forth for use in the transient analysis.

The five transient cases were run with a radial constraint applied along the entire boreriding surface of both the sabot and armature. Stress plots of the projectile at the time of maximum equivalent stress are shown in Figures 12–16 for the five acceleration loading profiles. Neither the sabot nor penetrator reach values exceeding their respective yield values. The results of the transient analysis show agreement within 2% of the calculated stress values for the quasi-static analysis runs. Again, it is noted that removal of the radial displacement constraint would likely result in stresses exceeding the sabot material's yield strength.

Depicted in Figures 16–21 are plots of the stress time history of an element located in the center of the penetrator. These plots reflect the various rise and fall times of the acceleration profiles used as input. It is noticed that every trace exhibits an oscillatory response following the attainment of peak stress. To determine whether this is a transient effect due to the unloading of the current through the projectile or an artifact of element hour-glassing, it is necessary to calculate the transit time, T. This transit time is defined by

$$T = \frac{\text{total penetrator length traversed}}{\text{wave speed of the material}} \quad .$$

The wave speed for a material is expressed as $\sqrt{E/\rho}$, where E is the elastic modulus of the material and ρ is its density. For the tungsten penetrator, this results in

$$T = \frac{(2)\ (3.865\ \text{in})}{\sqrt{(44\times10^{6}\ \text{psi}) \Big/ \left(\frac{0.638\ \text{lbm/in}^{3}}{386.4}\right)}} = 47.3\mu\text{s} \quad .$$

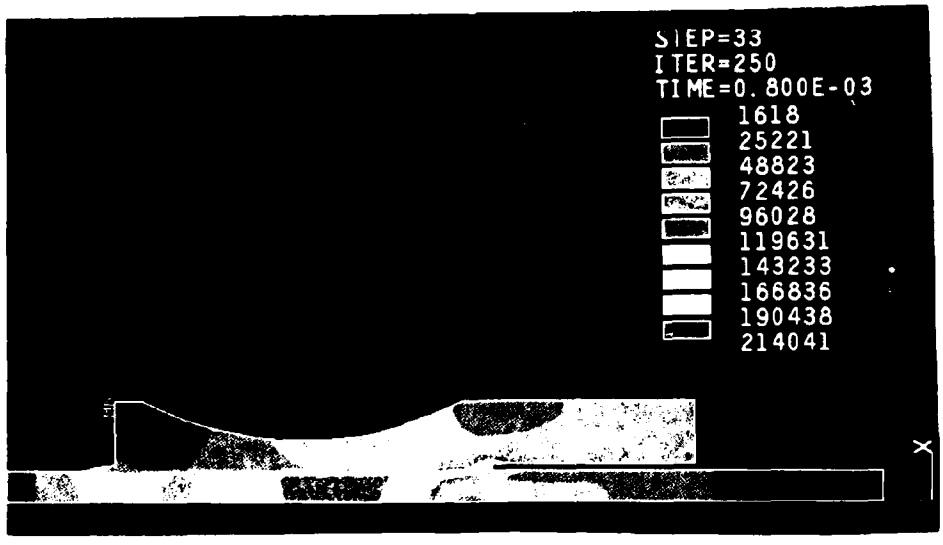
STEP=33
ITER=250
TIME=0.800E-03
1618
25221
48823
72426
96028
119631
143233
166836
190438
214041
X

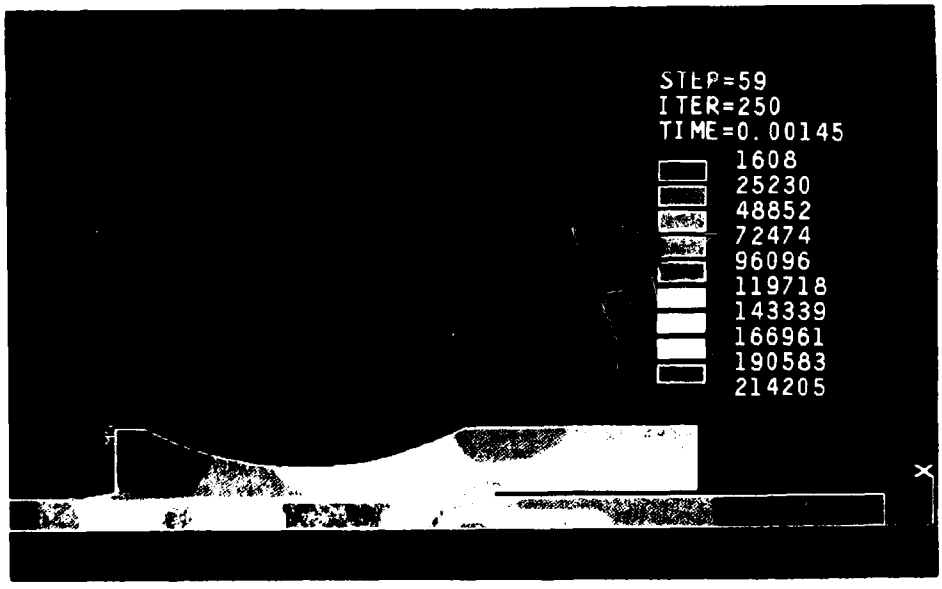
STEP=59
ITER=250
TIME=0.00145
1608
25230
48852
72474
96096
119718
143339
166961
190583
214205
X

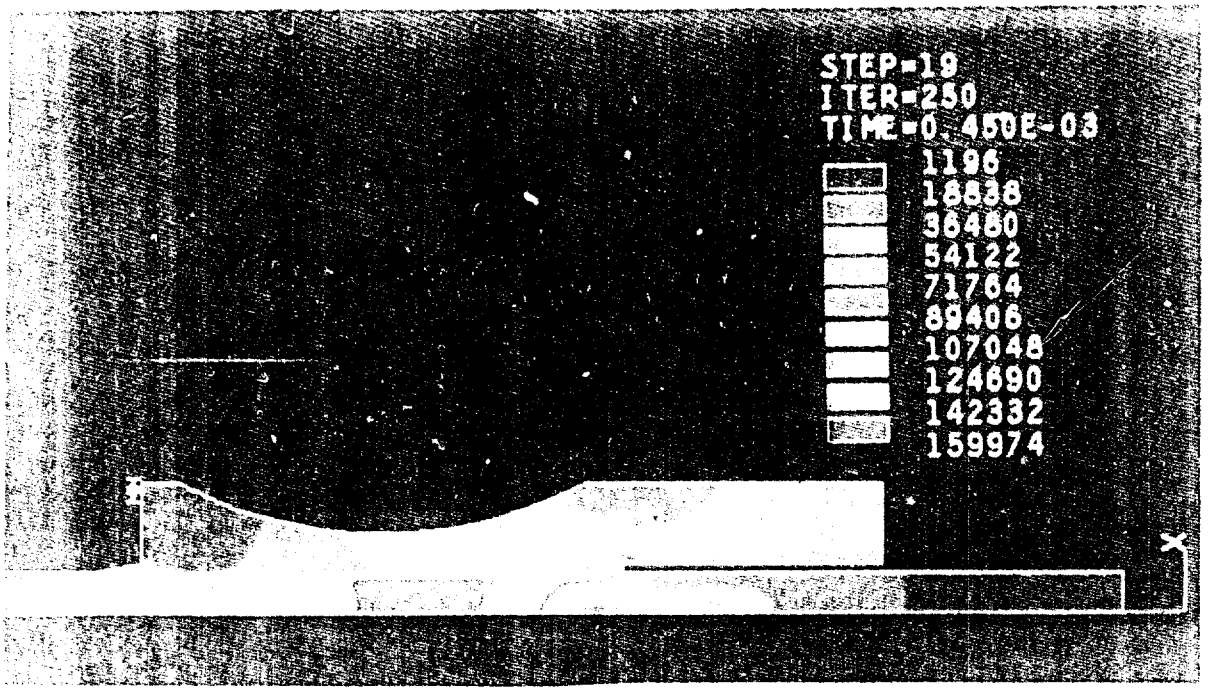
STEP=19
ITER=250
TIME=0.450E-03
1196
18838
36480
54122
71764
89406
107048
124690
142332
159974
X

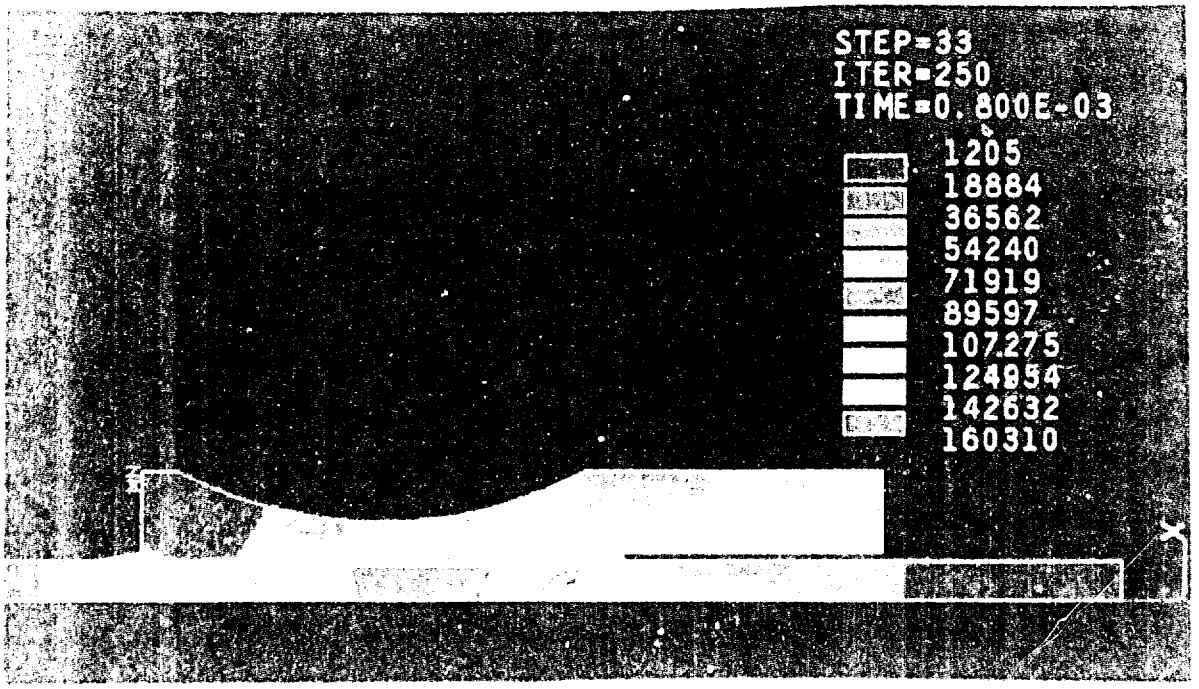
STEP=33
ITER=250
TIME=0.800E-03
1205
18884
36562
54240
71919
89597
107275
124954
142632
160310
X

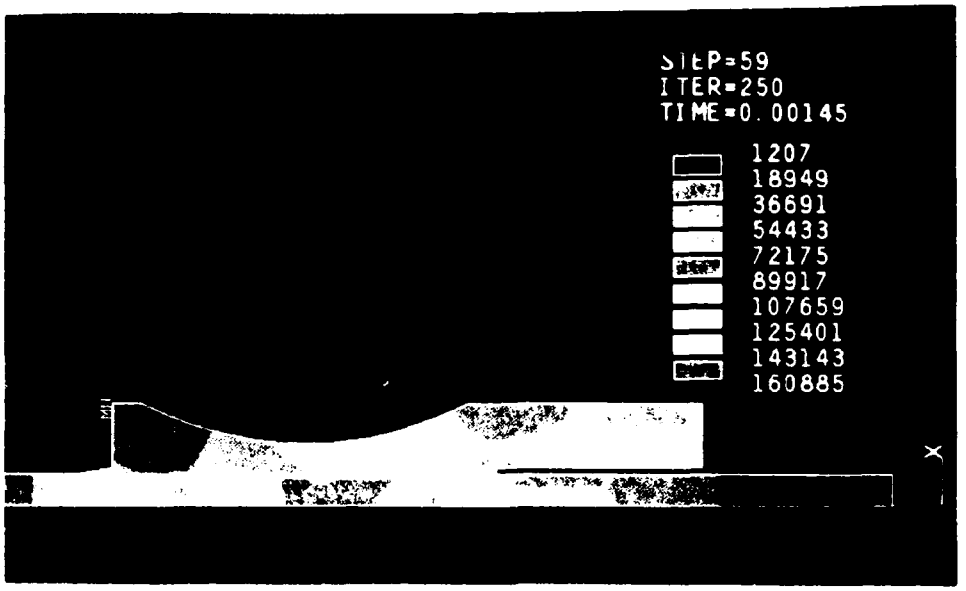
STEP=59
ITER=250
TIME=0.00145
1207
18949
36691
54433
72175
89917
107659
125401
143143
160885

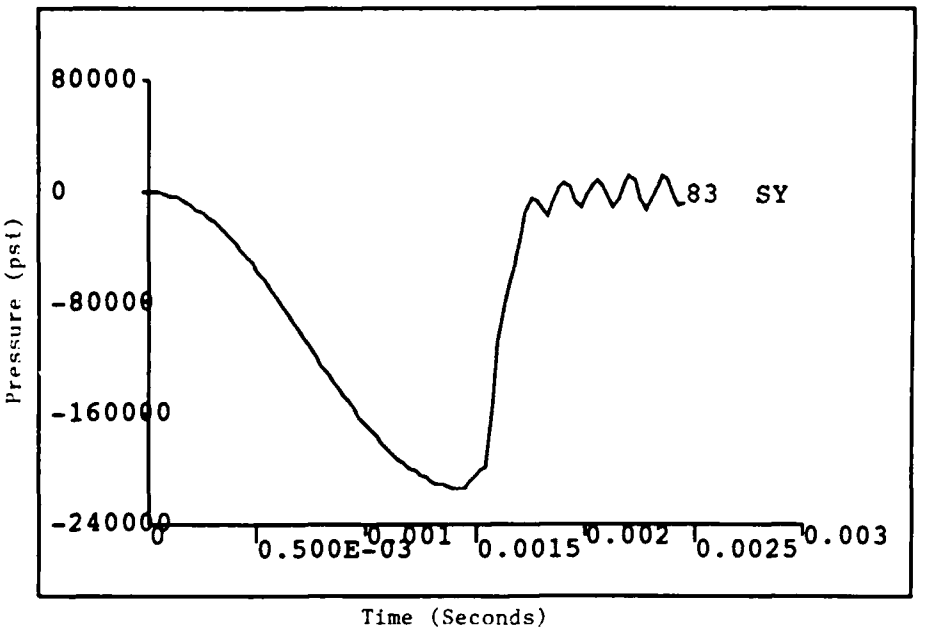

Figure 18. Stress history of penetrator element subjected to accelerator case 2.

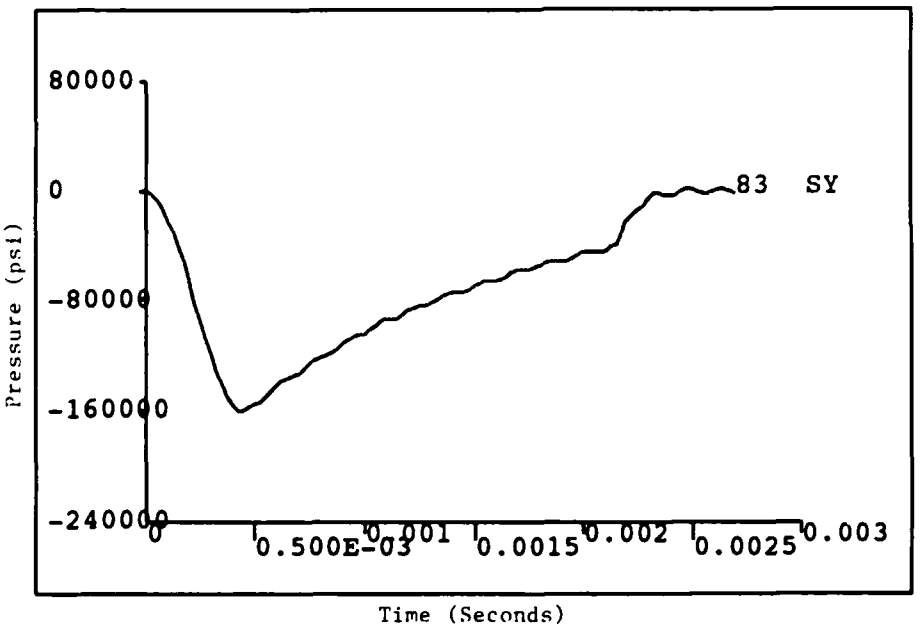

Figure 19. Stress history of penetrator element subjected to acceleration case 3.

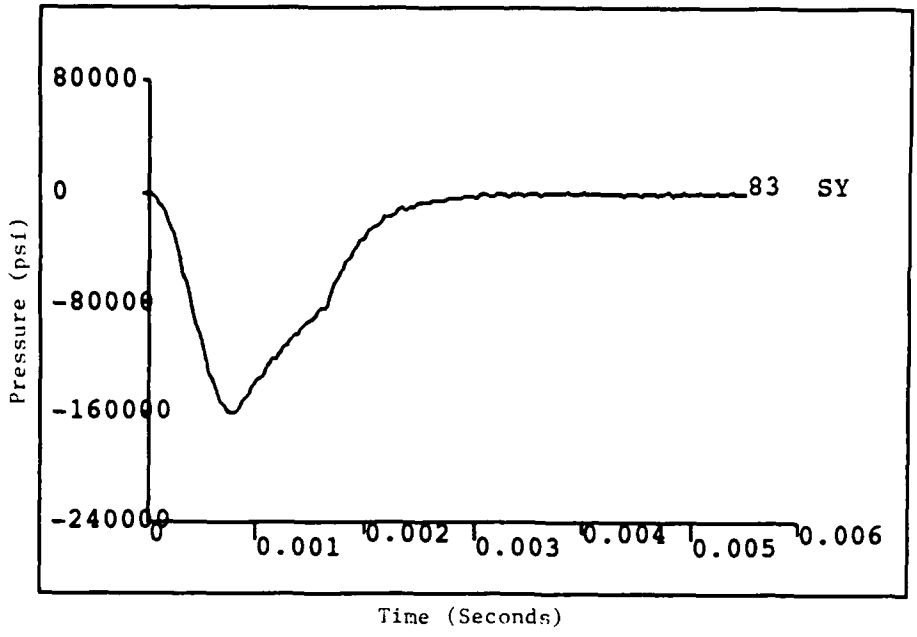

Figure 20. Stress history of penetrator element subjected to acceleration case 4.

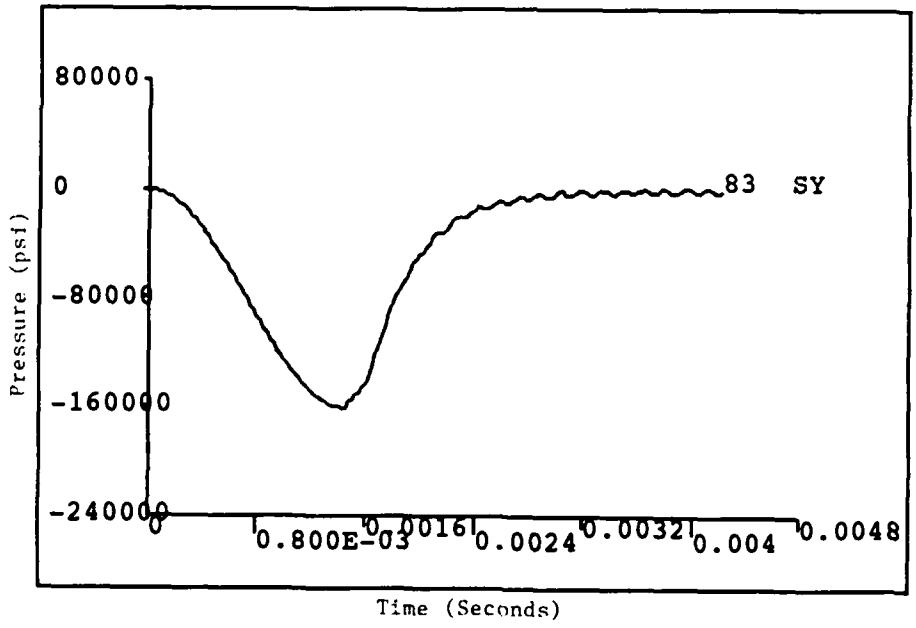

Figure 21. Stress history of penetrator element subjected to acceleration case 5.

A comparison of the penetrator's calculated wave transit time vs. the response frequency of the rod seen in Figures 16–21, shows that the oscillations are much slower than the transit time and are thus not attributable to the transient dynamics of the unloading of the current pulse. It is believed that the fluctuations in stress levels are a result of element hour-glassing effects.

6. CONCLUSIONS

This work laid out a methodology for the analysis of EM projectiles using conventional FE techniques. A pressure loading on the rear of the armature was utilized to simulate the magnitude of the true electromagnetic body force. An improvement to the technique would be to incorporate the FE capability of applying forces directly to internal nodes of the modeled structure. There are currently several codes written or under development which predict the current distribution through the armature (Powell et al. 1993) whose results could be applied as input loads for the structural analysis. However, the technique as demonstrated here provides a relatively good approximation of the loading conditions and is rather easy to implement.

The analysis effort points out the importance of applying realistic boundary conditions. Utilizing a radial boundary constraint as typically done for the analysis of projectiles in conventional gun systems can lead to a faulty design being deemed acceptable. Obviously, such an erroneous conclusion could be catastrophic. The separation of the rails inherent in the EM guns is of concern to projectile designers and should be addressed in future analysis work.

Finally, while the transient analysis performed on the projectile during this investigation produced little difference compared to the quasi-static cases, it is important that the EM projectile designer go through the process of examining the dynamic loading effects. This becomes especially true as the rod length is increased and the rise time is reduced, resulting in insufficient time for the oscillations of any stress waves to decay away. Longer rods mean increased transit times which may lead to amplification of stresses as they approach the rise time of the acceleration profile. While Bender's work with bare rods has shown rise times in excess of five times to be of sufficient length to ignore the transient wave effects, others working with saboted projectiles typically use a factor of ten between the rise time and transit time before ignoring the wave phenomenon (Hopkins 1993).

INTENTIONALLY LEFT BLANK.

7. REFERENCES

Bannister, K. A., L. Burton, W. H. Drysdale. "Structural Design Issues for Electromagnetic Projectiles." BRL-TR-3299, U.S. Army Ballistic Research Laboratory, Aberdeen Proving Ground, MD, December 1991.

Bender, J. M. "Stress Waves Through Projectile Joints and Interfaces." BRL-TR-2980, U.S. Army Ballistic Research Laboratory, Aberdeen Proving Ground, MD, January 1989.

DeSalvo, G. J., and R. W. Gorman. "ANSYS Engineering Analysis System User's Manual - Revision 4.4." Swanson Analysis Systems, Inc., Houston, PA, May 1989.

Hopkins, D. Private communication. U.S. Army Research Laboratory, Aberdeen Proving Ground, MD, June 1993.

Jamison, K., and H. Burden. "Measurements of Plasma Properties from a Large Bore, Plasma Armature Railgun." IEEE Transactions on Magnetics, vol. 25, no. 1, pp. 256–261, January 1989.

Mongeau, P. P. "Inductively Commutated Coilguns." Fifth Symposium on EML Technology, Destin, FL, April 1990.

Powell, J. D., W. H. Drysdale, B. P. Burns, and A. E. Zielinski. "A Survey of Codes for Modeling Electromagnetic Launch." ARL-MR-64, U.S. Army Research Laboratory, Aberdeen Proving Ground, MD, May 1993.

Powell, J. D., D. J. Walbert, and A. E. Zielinski. "Two-Dimensional Model for Current and Heat Transport in Solid-Armature Railguns." ARL-TR-74, U.S. Army Research Laboratory, Aberdeen Proving Ground, MD, February 1993.

Price, J. H., C. W. G. Filcher, M. W. Ingram, D. E. Perkins, and D. R. Peterson. "Results of Monolithic Solid Armature Tests in a Railgun." PN-134, Center for Electromechanics, The University of Texas at Austin, Austin, TX, November 1987.

Sorensen, B. R. "Design and Analysis of Kinetic Energy Projectiles Using Finite Element Optimization." BRL-TR-3289, U.S. Army Ballistic Research Laboratory, Aberdeen Proving Ground, MD, November 1991.

Zielinski, A. E. "Saboted Rod Projectile For Electromagnetic Launch." Proceedings of the 12th International Symposium on Ballistics, San Antonio, TX, November 1990.

Zielinski, A. E. "Design Limitations for Small Caliber Electromagnetic Saboted Rod Projectiles." IEEE Transactions on Magnetics, vol. 27, no. 1, pp. 521–526, January 1991.

Zielinski, A. E. Private communication, U.S. Army Research Laboratory, Aberdeen Proving Ground, MD, June 1992.

Zielinski, A. E. "A Projectile-Oriented, Design Study for a Cannon-Caliber Electromagnetic Launcher." IEEE Transactions on Magnetics, vol. 29, no. 1, pp. 889–894, January 1993.

Zielinski, A., J. Kezerian, and J. Beno. "An Interferometric Measurement Technique for Railgun Structures." BRL-MR-3646, U.S. Army Ballistic Research Laboratory, Aberdeen Proving Ground, MD, January 1988.

APPENDIX:

DENSITY CALCULATION OF MODIFIED ARMATURE CONFIGURATION

INTENTIONALLY LEFT BLANK.

The EM projectile analyzed in this investigation does not have an axisymmetric cross section as seen from Figure 2. It was desired to avoid having to use a three-dimensional element model to simplify both the construction of the projectile geometry and the time required to solve the problem. The adopted approach was to model the rear armature shown below (Figure A-1) as a cylinder with an equivalent mass. Since only the rear 0.9 inch (2.29 cm) of the armature is replaced by a cylinder of the same length, there is no need to worry about a shift in the center of gravity.

The first step was to calculate the weight of the actual armature configuration. This required a determination of the volume, and in turn, the area of the cross section. The area was determined by subtracting the area of the penetrator, A_{rod}, and the area of above the flat, A_{seg}, from the area of the full cylinder, A_{full}, of radius 0.452 in (1.15 cm). The areas are calculated as

$$A_{full} = \frac{\pi R^2}{2} = \frac{\pi (0.452 \text{ in})^2}{2} = 0.321 \text{ in}^2$$

$$A_{rod} = \frac{\pi r^2}{2} = \frac{\pi (0.139 \text{ in})^2}{2} = 0.030 \text{ in}^2$$

$$A_{seg} = \frac{1}{2} R^2 (\text{rad } A - \sin A) = \frac{1}{2}(0.452 \text{ in})^2 (1.92 - 0.94) = 0.100 \text{ in}^2 ,$$

where rad A is the radian measure of angle A shown in Figure A-1 (Marks 1951).[†] Thus,

$$m_{actual} = [A_{full} - A_{rod} - A_{seg}] L \rho_{actual} , \qquad \text{(A-1)}$$

where L is the 0.9-in length and ρ_{actual} is the density of aluminum, 0.98 lb/in^3. Substitution of values into equation A-1 yields a mass of 0.0168 lb (0.00076 kg). Division of this mass by the volume of the full cylinder minus the rod volume will provide a density for the modified armature geometry. That is,

[†] Marks, L. S. Mechanical Engineers' Handbook. New York: McGraw-Hill Book Company, Inc., 1951.

$$\rho_{fudge} = \frac{mass}{(A_{full} - A_{rod})\, L} \quad . \qquad \text{(A-2)}$$

Again, substitution of values into equation A-2 gives a value of 0.064 lb/in^3 (1,770 kg/m^3) which is used for the armature material in the geometry model.

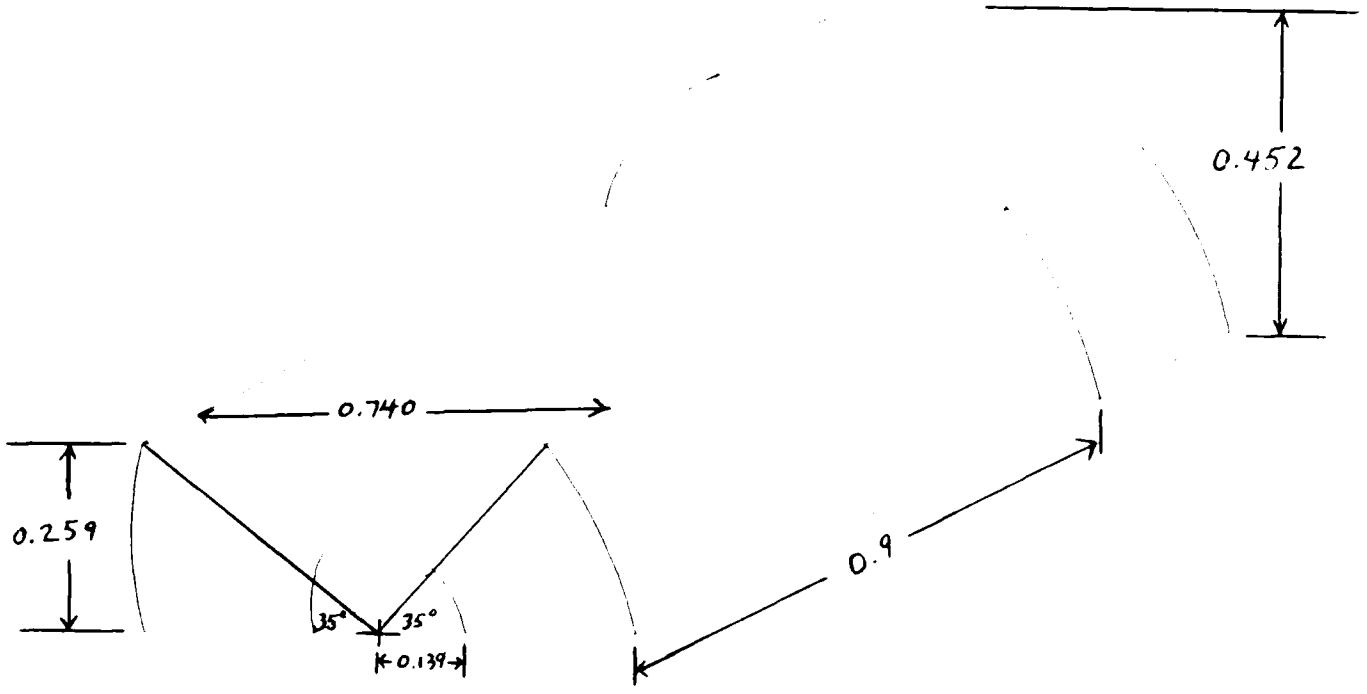

Figure A-1. Sketch of aft end armature.

INTENTIONALLY LEFT BLANK.

No. of Copies	Organization
2	Administrator Defense Technical Info Center ATTN: DTIC-DDA Cameron Station Alexandria, VA 22304-6145
1	Commander U.S. Army Materiel Command ATTN: AMCAM 5001 Eisenhower Ave. Alexandria, VA 22333-0001
1	Director U.S. Army Research Laboratory ATTN: AMSRL-OP-CI-AD, Tech Publishing 2800 Powder Mill Rd. Adelphi, MD 20783-1145
1	Director U.S. Army Research Laboratory ATTN: AMSRL-OP-CI-AD, Records Management 2800 Powder Mill Rd. Adelphi, MD 20783-1145
2	Commander U.S. Army Armament Research, Development, and Engineering Center ATTN: SMCAR-IMI-I Picatinny Arsenal, NJ 07806-5000
2	Commander U.S. Army Armament Research, Development, and Engineering Center ATTN: SMCAR-TDC Picatinny Arsenal, NJ 07806-5000
1	Director Benet Weapons Laboratory U.S. Army Armament Research, Development, and Engineering Center ATTN: SMCAR-CCB-TL Watervliet, NY 12189-4050
1	Director U.S. Army Advanced Systems Research and Analysis Office (ATCOM) ATTN: AMSAT-R-NR, M/S 219-1 Ames Research Center Moffett Field, CA 94035-1000

No. of Copies	Organization
1	Commander U.S. Army Missile Command ATTN: AMSMI-RD-CS-R (DOC) Redstone Arsenal, AL 35898-5010
1	Commander U.S. Army Tank-Automotive Command ATTN: AMSTA-JSK (Armor Eng. Br.) Warren, MI 48397-5000
1	Director U.S. Army TRADOC Analysis Command ATTN: ATRC-WSR White Sands Missile Range, NM 88002-5502
(Class. only) 1	Commandant U.S. Army Infantry School ATTN: ATSH-CD (Security Mgr.) Fort Benning, GA 31905-5660
(Unclass. only) 1	Commandant U.S. Army Infantry School ATTN: ATSH-WCB-O Fort Benning, GA 31905-5000
1	WL/MNOI Eglin AFB, FL 32542-5000
	Aberdeen Proving Ground
2	Dir, USAMSAA ATTN: AMXSY-D AMXSY-MP, H. Cohen
1	Cdr, USATECOM ATTN: AMSTE-TC
1	Dir, ERDEC ATTN: SCBRD-RT
1	Cdr, CBDA ATTN: AMSCB-CII
1	Dir, USARL ATTN: AMSRL-SL-I
5	Dir, USARL ATTN: AMSRL-OP-CI-B (Tech Lib)

No. of Copies	Organization
11	Director Benet Weapons Laboratory U.S. Army Armament Research, Development, and Engineering Center ATTN: SMCAR-CCB, F. Heizer J. Keane T. Allen J. Vasilakis G. Friar J. Zweig T. Simkins V. Montvori J. Wrzochalski G. D'Andrea R. Hasenbein Watervliet, NY 12189
1	Commander ATTN: SMCWV-QAE-Q, C. Howd Bldg. 44 Watervliet Arsenal Watervliet, NY 12189-4050
1	Commander ATTN: SMCWV-SPM, T. McCloskey Bldg. 25/3, Watervliet Arsenal Watervliet, NY 12189-4050
5	Commander U.S. Army Armament Research, Development, and Engineering Center ATTN: SMCAR-CCH-T, S. Musalli P. Christian K. Fehsal N. Krasnow R. Carr Picatinny Arsenal, NJ 07806-5000
1	Commander U.S. Army Armament Research, Development, and Engineering Center ATTN: SMCAR-CCH-V, E. Fennell Picatinny Arsenal, NJ 07806-5000

No. of Copies	Organization
1	Commander U.S. Army Armament Research, Development, and Engineering Center ATTN: SMCAR-CCH, J. DeLorenzo Picatinny Arsenal, NJ 07806-5000
1	Commander U.S. Army Armament Research, Development, and Engineering Center ATTN: SMCAR-CC, J. Hedderich Picatinny Arsenal, NJ 07806-5000
1	Commander U.S. Army Armament Research, Development, and Engineering Center ATTN: SMCAR-CCH-P, J. Lutz Picatinny Arsenal, NJ 07806-5000
3	Commander U.S. Army Armament Research, Development, and Engineering Center ATTN: SMCAR-TD, R. Price V. Linder T. Davidson Picatinny Arsenal, NJ 07806-5000
1	Commander Production Base Modernization Activity U.S. Army Armament Research, Development, and Engineering Center ATTN: AMSMC-PBM-K Picatinny Arsenal, NJ 07806-5000
1	Commander U.S. Army Belvoir RD&E Center ATTN: STRBE-JBC, C. Kominos Fort Belvoir, VA 22060-5606
2	Commander U.S. Army Missile Command ATTN: AMSMI-RD, W. McCorkle AMSMI-RD-ST, P. Doyle Redstone Arsenal, AL 35898

No. of Copies	Organization
2	Commander U.S. Army Armament Research, Development, and Engineering Center ATTN: SMCAR-FSA-M, R. Botticelli F. Diorio Picatinny Arsenal, NJ 07806-5000
1	Commander U.S. Army Armament Research, Development, and Engineering Center ATTN: SMCAR-FSA, C. Spinelli Picatinny Arsenal, NJ 07806-5000
6	Commander U.S. Army Armament Research, Development, and Engineering Center ATTN: SMCAR-FSE, T. Gora E. Andricopoulos B. Knutelsky A. Graf J. Bennett C. Dunham Picatinny Arsenal, NJ 07806-5000
3	Project Manager Advanced Field Artillery System ATTN: COL Napoliello LTC A. Ellis G. DelCoco Picatinny Arsenal, NJ 07806-5000
1	Commander Watervliet Arsenal ATTN: SMCWV-QA-QS, K. Insco Watervliet, NY 12189-4050
2	Project Manager SADARM Picatinny Arsenal, NJ 07806-5000
2	Project Manager Tank Main Armament Systems ATTN: SFAE-AR-TMA, COL Hartline C. Kimker Picatinny Arsenal, NJ 07806-5000

No. of Copies	Organization
2	Project Manager Tank Main Armament Systems ATTN: SFAE-AR-TMA-MD, H. Yuen J. McGreen Picatinny Arsenal, NJ 07806-5000
2	Project Manager Tank Main Armament Systems ATTN: SFAE-AR-TMA-MS, R. Joinson D. Guziewicz Picatinny Arsenal, NJ 07806-5000
1	Project Manager Tank Main Armament Systems ATTN: SFAE-AR-TMA-MP, W. Lang Picatinny Arsenal, NJ 07806-5000
1	U.S. Army Research Laboratory Advanced Concepts and Plans ATTN: AMSRL-CP-CA, D. Snider 2800 Powder Mill Rd. Adelphi, MD 20783
1	U.S. Army Materiel Command ATTN: AMCSCI, R. Chait 5001 Eisenhower Ave. Alexandria, VA 22333-0001
2	PEO-Armaments ATTN: SFAE-AR-PM, D. Adams T. McWilliams Picatinny Arsenal, NJ 07806-5000
2	U.S. Army Research Office Dir., Math & Computer Sciences Div. ATTN: A. Crowson AMXRO-MCS, J. Chandra P.O. Box 12211 Research Triangle Park, NC 27709-2211
2	NASA Langley Research Center Mail Stop 266 ATTN: F. Barlett, Jr. AMSRL-VS, W. Elber Hampton, VA 23681-0001

No. of Copies | Organization

1 Commander
Wright-Patterson Air Force Base
ATTN: AFWAML, R. Kim
Dayton, OH 45433

2 Commander
DARPA
ATTN: J. Kelly
B. Wilcox
3701 North Fairfax Dr.
Arlington, VA 22203-1714

6 Director
U.S. Army Research Laboratory
Materials Technology Directorate
ATTN: AMSRL-MA-P,
L. Johnson
B. Halpin
T. Chou
AMSRL-MA-PA,
D. Granville
W. Haskell
AMSRL-MA-MA, G. Hagnauer
Watertown, MA 02172-0001

1 Naval Research Laboratory
Code 6383
ATTN: Dr. I. Wolock
Washington, DC 20375-5000

1 Office of Naval Research
Mechanical Division Code 1132-SM
ATTN: Y. Rajapakse
Arlington, VA 22217

2 David Taylor Research Center
ATTN: R. Rockwell
W. Phyillaier
Bethesda, MD 20054-5000

1 David Taylor Research Center
Ship Structures and Protection Dept.
ATTN: J. Corrado, Code 1702
Bethesda, MD 20084

No. of Copies | Organization

4 Director
Lawrence Livermore National Laboratory
ATTN: R. Christensen
S. deTeresa
W. Feng
F. Magness
P.O. Box 808
Livermore, CA 94550

2 Pacific Northwest Laboratory
A Div of Batelle Memorial Inst.
Technical Information Section
ATTN: M. Smith
M.C.C. Bampton
P.O. Box 999
Richland, WA 99352

6 Director
Sandia National Laboratories
Applied Mechanics Dept.,
Division-8241
ATTN: C. Robinson
G. Benedetti
W. Kawahara
K. Perano
D. Dawson
P. Nielan
P.O. Box 969
Livermore, CA 94550-0096

1 Director
Los Alamos National Laboratory
ATTN: D. Rabern
MEE-13, Mail Stop J-576
P.O. Box 1633
Los Alamos, NM 87545

1 The University of Texas at Austin
Center for Electromechanics
ATTN: J. Price
10100 Burnet Rd.
Austin, TX 78758-4497

2 Virginia Polytechnical Institute
and State University, Dept. of ESM
ATTN: M. W. Hyer
K. L. Reifsnider
Blacksburg, VA 24061-0219

No. of Copies	Organization
2	University of Dayton Research Institute ATTN: R. Y. Kim A. K. Roy 300 College Park Ave. Dayton, OH 45469-0168
1	University of Dayton ATTN: J. M. Whitney 300 College Park Ave. Dayton, OH 45469-0240
1	Drexell University ATTN: A. S. D. Wang 32nd and Chestnut Sts. Philadelphia, PA 19104
1	Purdue University School of Aeronautics and Astronautics ATTN: C. T. Sun West Lafayette, IN 47907-1282
1	University of Kentucky ATTN: L. Penn 763 Anderson Hall Lexington, KY 40506-0046
3	University of Delaware Center for Composite Materials ATTN: J. Gillespe B. Pipes M. Santare 201 Spencer Laboratory Newark, DE 19716
2	North Carolina State University Civil Engineering Department ATTN: W. Rasdorf L. Spainhour P.O. Box 7908 Raleigh, NC 27696-7908
1	University of Utah Dept. of Mechanical and Industrial Engineering ATTN: S. Swanson Salt Lake City, UT 84112

No. of Copies	Organization
1	Stanford University Dept. of Aeronautics and Aeroballistics Durant Building ATTN: S. Tsai Stanford, CA 94305
1	Pennsylvania State University ATTN: R. S. Engle 245 Hammond Bldg. University Park, PA 16801
1	Pennsylvania State University ATTN: D. W. Jensen 223-N Hammond University Park, PA 16802
1	Pennsylvania State University ATTN: R. McNitt 227 Hammond Building University Park, PA 16802
1	UCLA MANE Dept., Engineering IV ATTN: H. T. Hahn Los Angeles, CA 90024-1597
1	University of Illinois at Urbana-Champaign National Center for Composite Materials Research 216 Talbot Laboratory ATTN: J. Economy 104 S. Wright St. Urbana, IL 61801
1	IAP Research, Inc. ATTN: A. Challita 2763 Culver Ave. Dayton, OH 45429
2	Olin Corporation Flinchbaugh Division ATTN: E. Steiner B. Stewart P.O. Box 127 Red Lion, PA 17356

No. of Copies	Organization
1	Olin Corporation ATTN: L. Whitmore 10101 9th St., North St. Petersburg, FL 33702
3	Alliant Techsystems, Inc. ATTN: C. Candland J. Bode K. Ward 5901 Lincoln Dr. Minneapolis, MN 55346-1674
1	Alliant Techsystems, Inc. Precision Armaments Systems Group 7225 Northland Dr. Brooklyn Park, MN 55428
1	Chamberlain Manufacturing Corporation Research and Development Division ATTN: T. Lynch 550 Esther St. P.O. Box 2335 Waterloo, IA 50704
1	Custom Analytical Engineering Systems, Inc. ATTN: A. Alexander Star Route, Box 4A Flintstone, MD 21530
2	Institute for Advanced Technology ATTN: T. Kiehne H. Fair 4030-2 W. Braker La. Austin, TX 78759
2	Kaman Sciences Corporation ATTN: D. Elder T. Hayden P.O. Box 7463 Colorado Springs, CO 80933
3	LORAL/Vought Systems ATTN: G. Jackson K. Cook L. L. Hadden 1701 W. Marshall Dr. Grand Prairie, TX 75051

No. of Copies	Organization
1	Interferometrics, Inc. ATTN: R. Larriva, Vice President 8150 Leesburg Pike Vienna, VA 22100
1	ARMTEC Defense Products ATTN: S. Dyer 85-901 Ave. 53 P.O. Box 848 Coachella, CA 92236
	Aberdeen Proving Ground
1	Chief, AMSRL-SL-BE
1	Chief, AMSRL-WT-WC
3	AMSRL-WT-WB, W. D'Amico A. Zielinski J. Powell
2	AMSRL-WT-TC, Chief R. Coates
1	AMSRL-WT-TA, Chief
19	AMSRL-WT-PD, Chief W. Drysdale K. Bannister T. Bogetti J. Bender J. Ford R. Murray R. Kirkendall T. Erline D. Hopkins S. Wilkerson R. Kaste L. Burton J. Tzeng AMSRL-WT-PE, Chief AMSRL-WT-PA, Chief AMSRL-WT-PC, Chief AMSRL-WT-PD, Chief AMSRL-WT-PB, Chief

No. of Copies	Organization
	Adelphi
9	Dir, U.S. Army Research Laboratory ATTN: AMSRL-WT-PD (ALC), A. Abrahamian K. Barnes M. Berman H. Davison A. Frydman T. Li W. McIntosh E. Szymanski H. Watkins

INTENTIONALLY LEFT BLANK.

USER EVALUATION SHEET/CHANGE OF ADDRESS

This Laboratory undertakes a continuing effort to improve the quality of the reports it publishes. Your comments/answers to the items/questions below will aid us in our efforts.

1. ARL Report Number ARL-TR-214 Date of Report September 1993

2. Date Report Received _____

3. Does this report satisfy a need? (Comment on purpose, related project, or other area of interest for which the report will be used.) _____

4. Specifically, how is the report being used? (Information source, design data, procedure, source of ideas, etc.) _____

5. Has the information in this report led to any quantitative savings as far as man-hours or dollars saved, operating costs avoided, or efficiencies achieved, etc? If so, please elaborate. _____

6 General Comments. What do you think should be changed to improve future reports? (Indicate changes to organization, technical content, format, etc.) _____

CURRENT ADDRESS

_____
Organization

_____
Name

_____
Street or P.O. Box No.

_____
City, State, Zip Code

7. If indicating a Change of Address or Address Correction, please provide the Current or Correct address above and the Old or Incorrect address below.

OLD ADDRESS

_____
Organization

_____
Name

_____
Street or P.O. Box No.

_____
City, State, Zip Code

(Remove this sheet, fold as indicated, tape closed, and mail.)

(DO NOT STAPLE)

DEPARTMENT OF THE ARMY

OFFICIAL BUSINESS

BUSINESS REPLY MAIL
FIRST CLASS PERMIT No 0001, APG, MD

Postage will be paid by addressee

Director
U.S. Army Research Laboratory
ATTN: AMSRL-OP-CI-B (Tech Lib)
Aberdeen Proving Ground, MD 21005-5066

NO POSTAGE
NECESSARY
IF MAILED
IN THE
UNITED STATES